Electronic Supplementary Information (ESI)

For

Bis-heteroleptic Ru(II) Polypyridine Complex-Based Luminescent Probes for Nerve Agent Simulant and Organophosphate Pesticide

Bhaskar Sen,[a] Monosh Rabha,[a] Sanjoy Kumar Sheet,[a] Debaprasad Koner,[b] Nirmalendu Saha,[b] Snehadrinarayan Khatua*[a]

[a]*Centre for Advanced Studies, Department of Chemistry, North Eastern Hill University, Shillong, Meghalaya 793022, India.*

[b]*Department of Zoology, North Eastern Hill University, Shillong, Meghalaya 793022, India.*

*Email: *snehadri@gmail.com*; *skhatua@nehu.ac.in*

Table of Contents **Page no**

Chart S1. List of Compounds used in this study

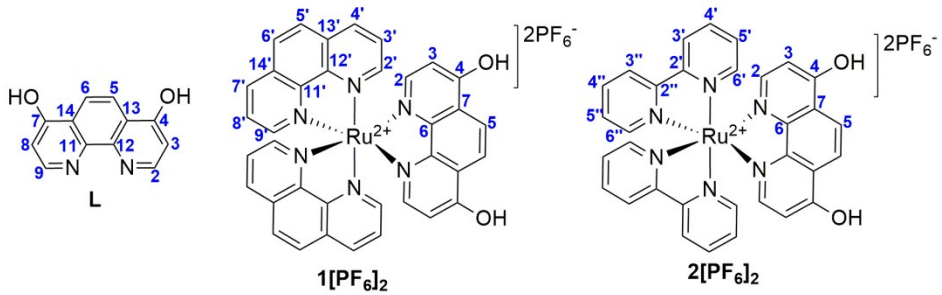

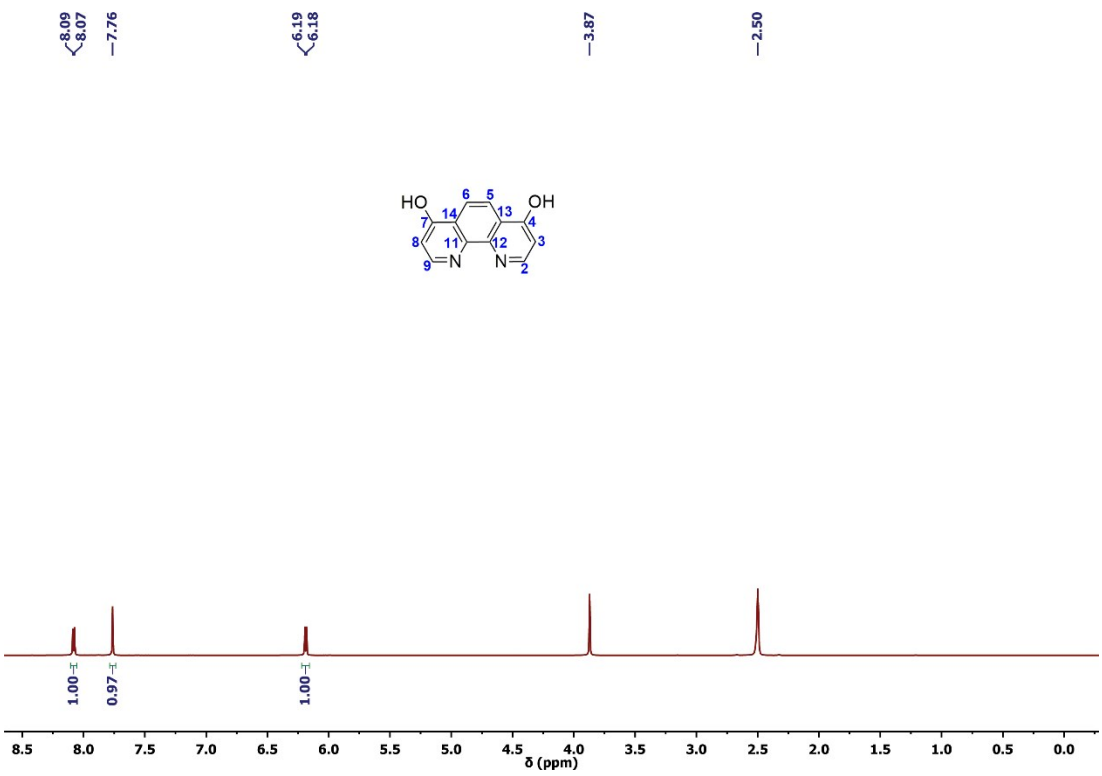

Figure S1. ^{1}H NMR spectrum of **L** in DMSO-d_6 : D_2O (25:1; v/v; in the presence of 0.25 mM NaOH).

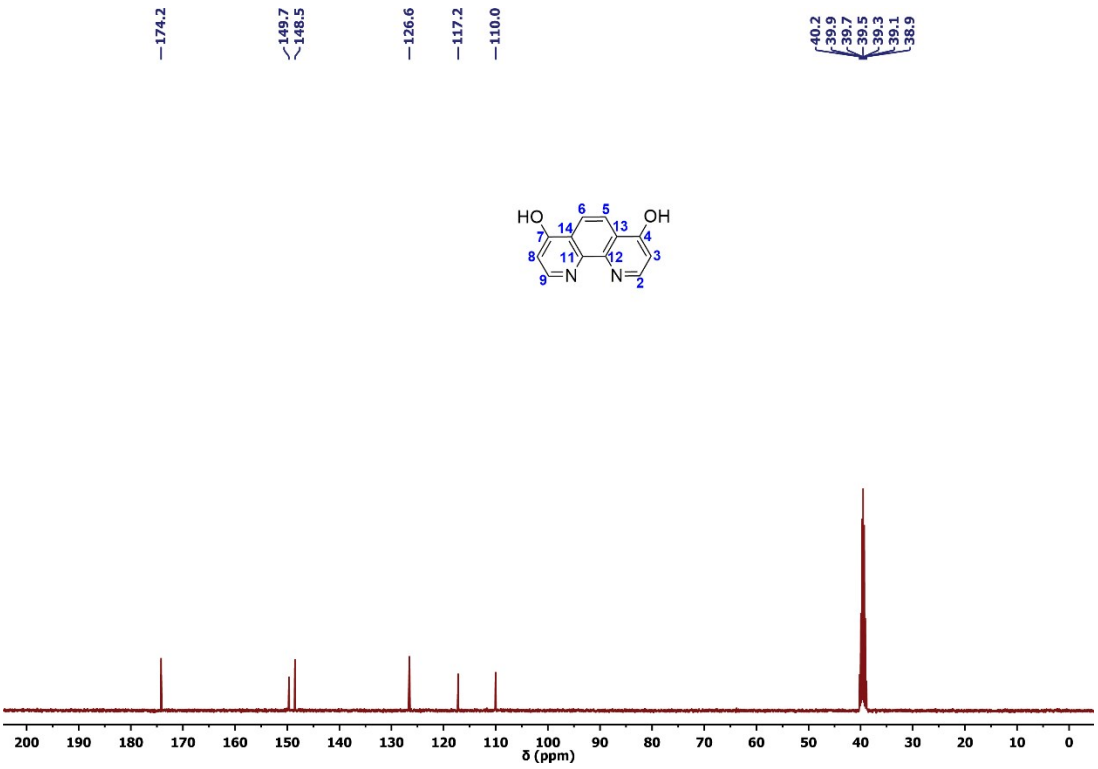

Figure S2. ^{13}C NMR spectrum of **L** in DMSO-d_6 : D_2O (25:1; v/v; in presence of 0.25 mM NaOH).

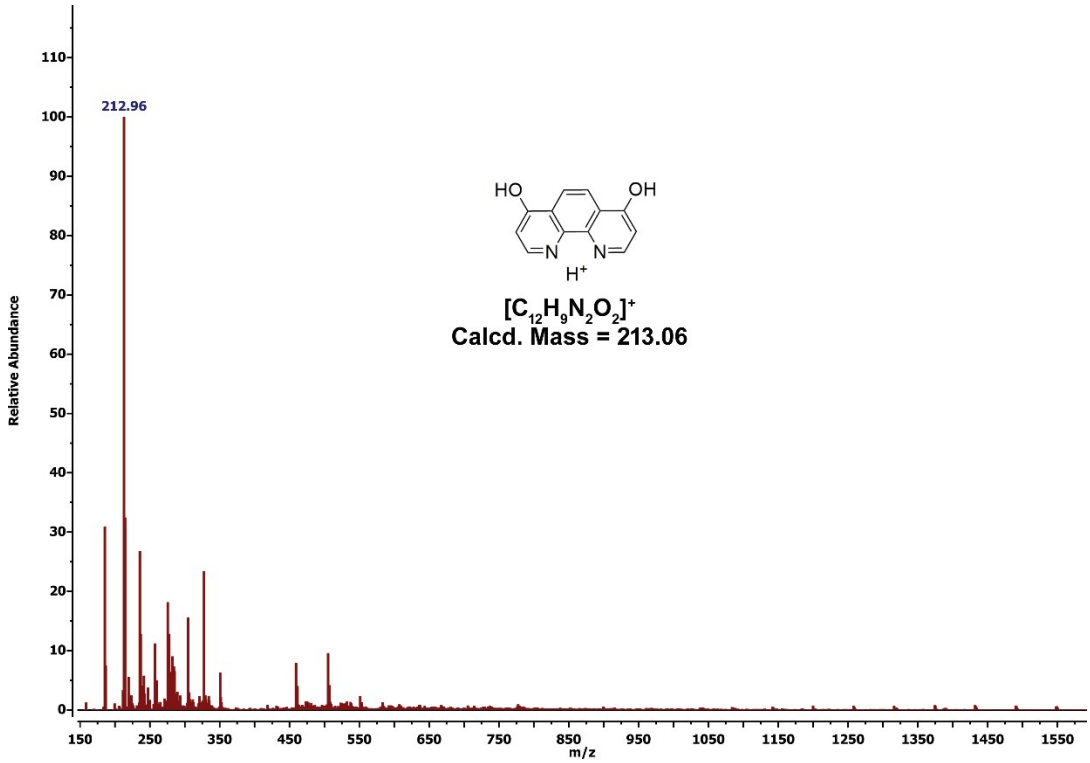

Figure S3. ESI-mass spectrum of **L** in methanol.

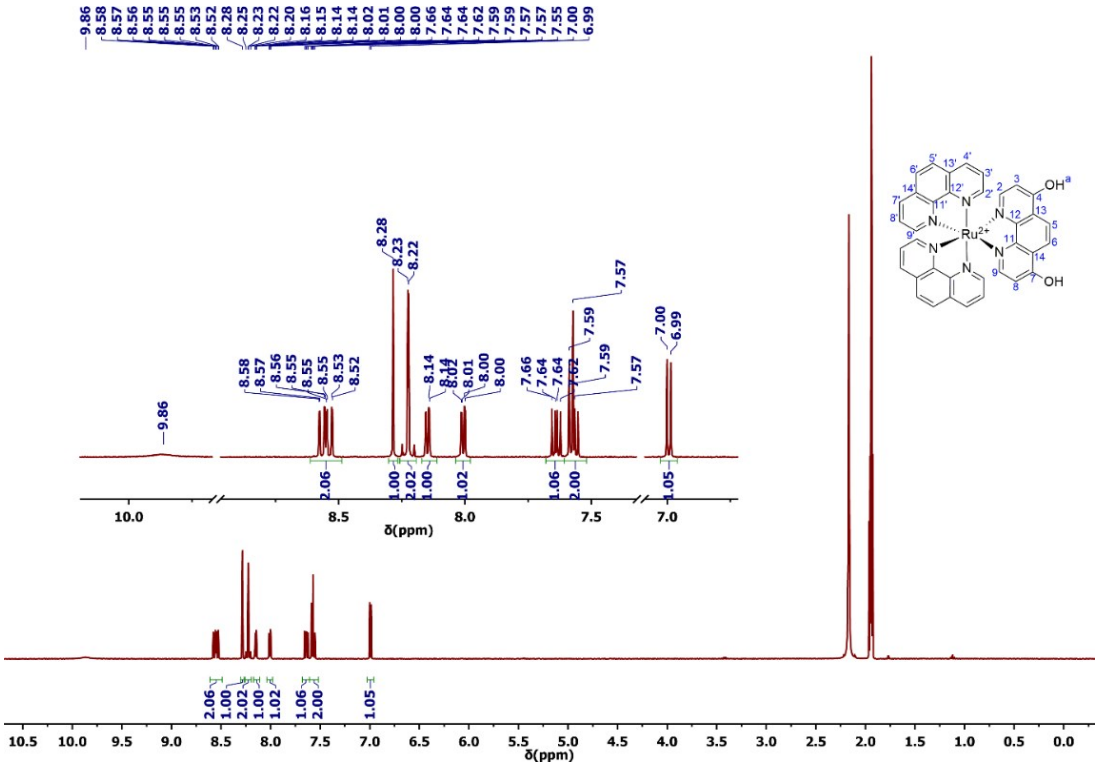

Figure S4. ^{1}H NMR spectrum of **1[PF$_6$]$_2$** in CD_3CN.

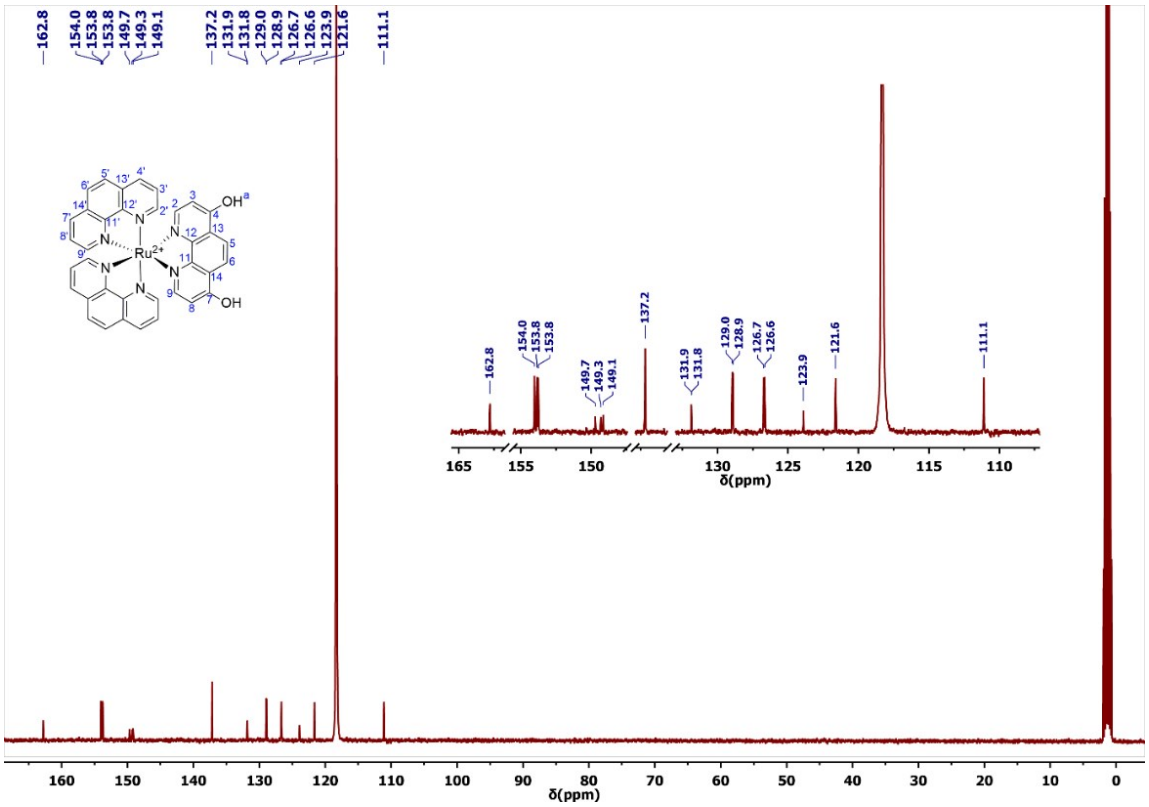

Figure S5. ^{13}C NMR spectrum of **1[PF$_6$]$_2$** in CD$_3$CN.

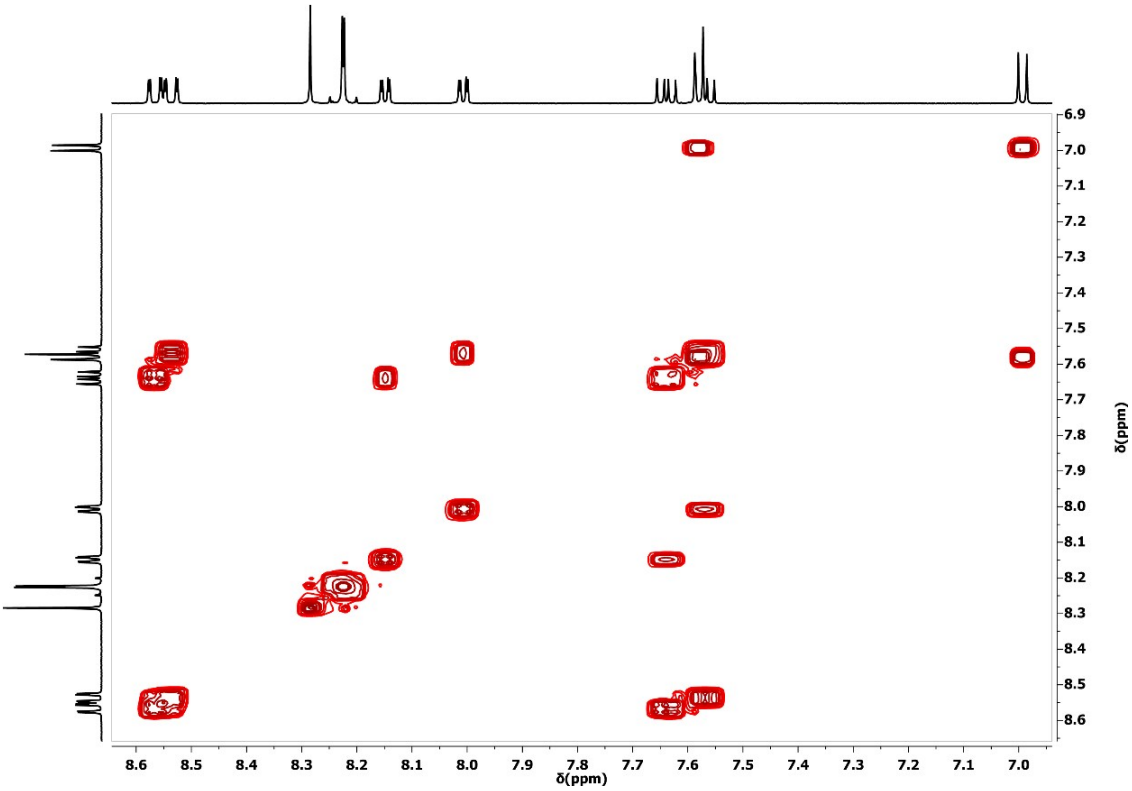

Figure S6. Partial ^{1}H-^{1}H COSY NMR spectrum of **1[PF$_6$]$_2$** in CD$_3$CN.

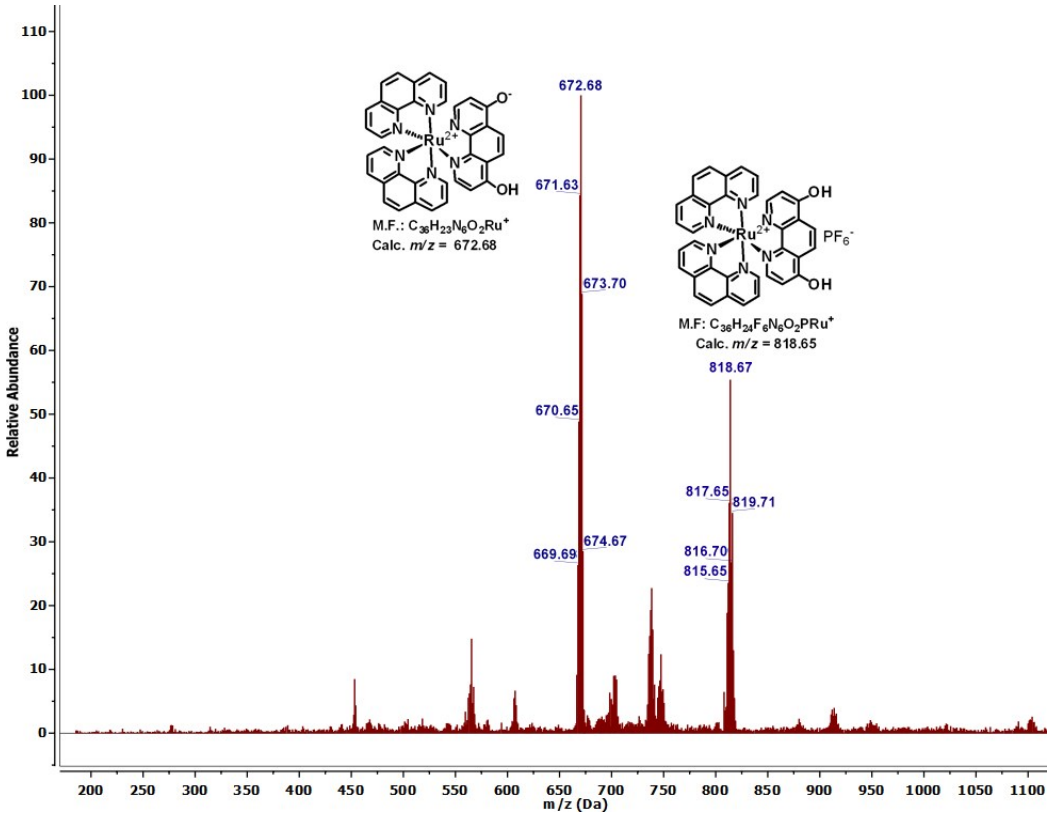

(a)

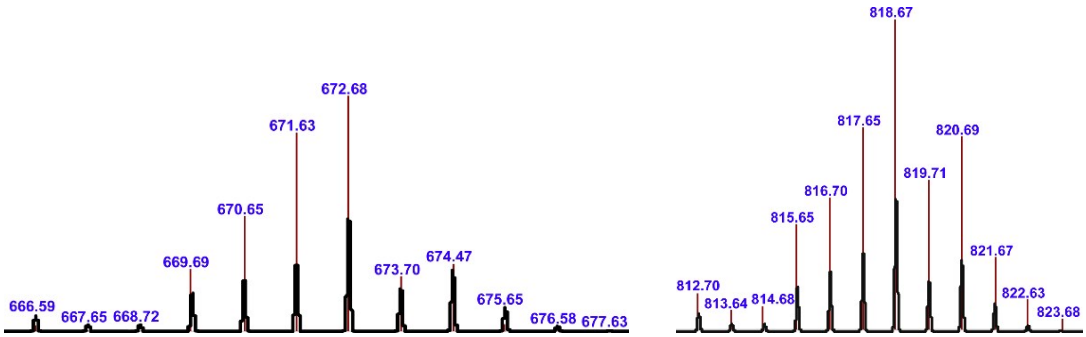

(b)

Figure S7. a) ESI-MS spectrum of **1[PF$_6$]$_2$** in CH_3CN and b) isotopic distribution of mass spectrum of **1[PF$_6$]$_2$** of experimentally obtained (red), simulated (black).

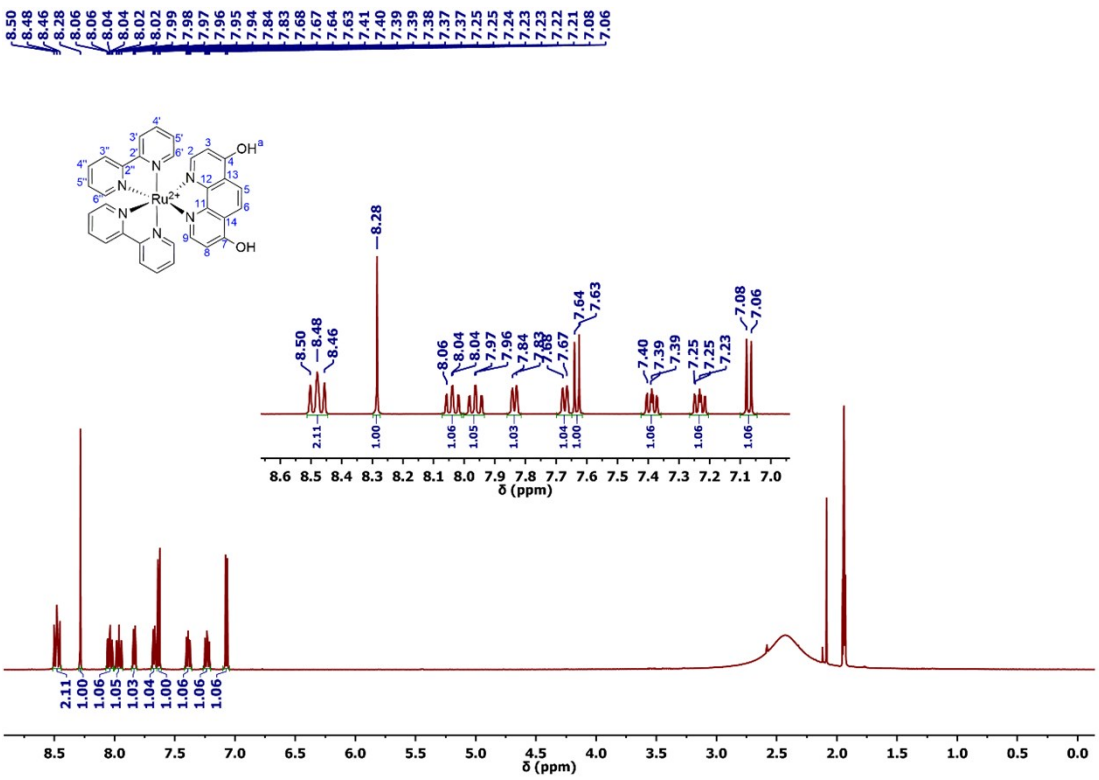

Figure S8. ^{1}H NMR spectrum of **2[PF$_6$]$_2$** in CD_3CN.

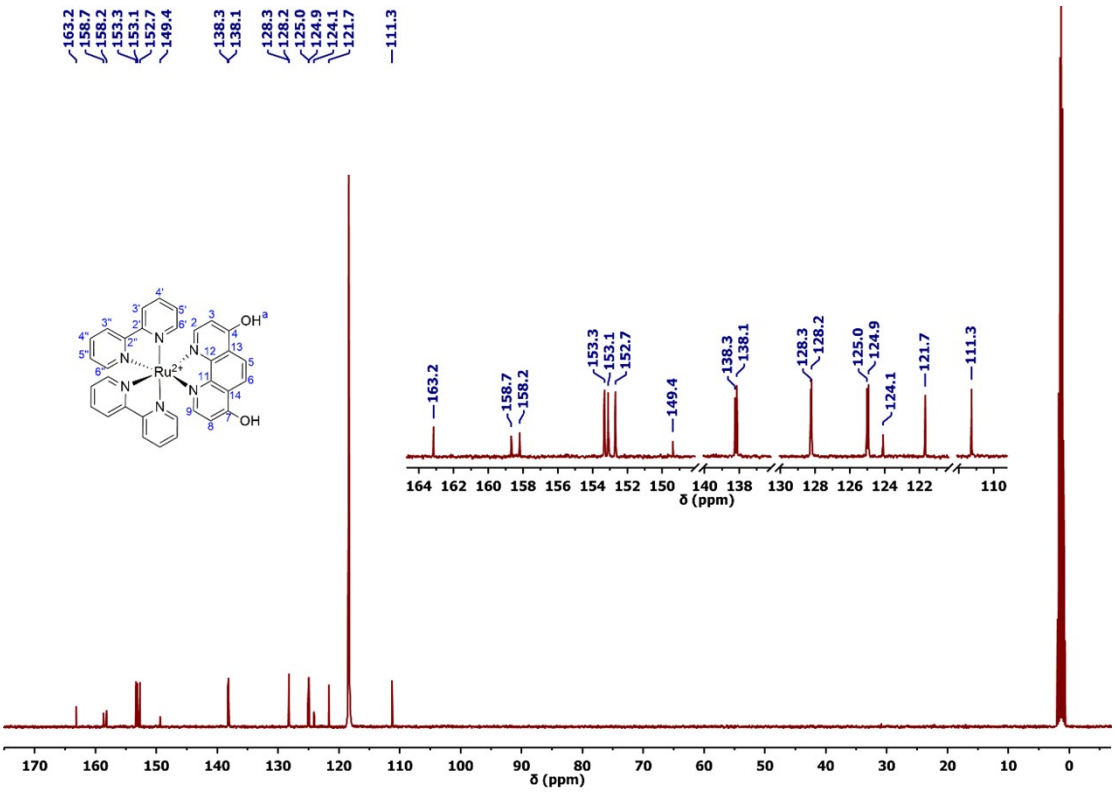

Figure S9. ^{13}C NMR spectrum of **2[PF$_6$]$_2$** in CD_3CN.

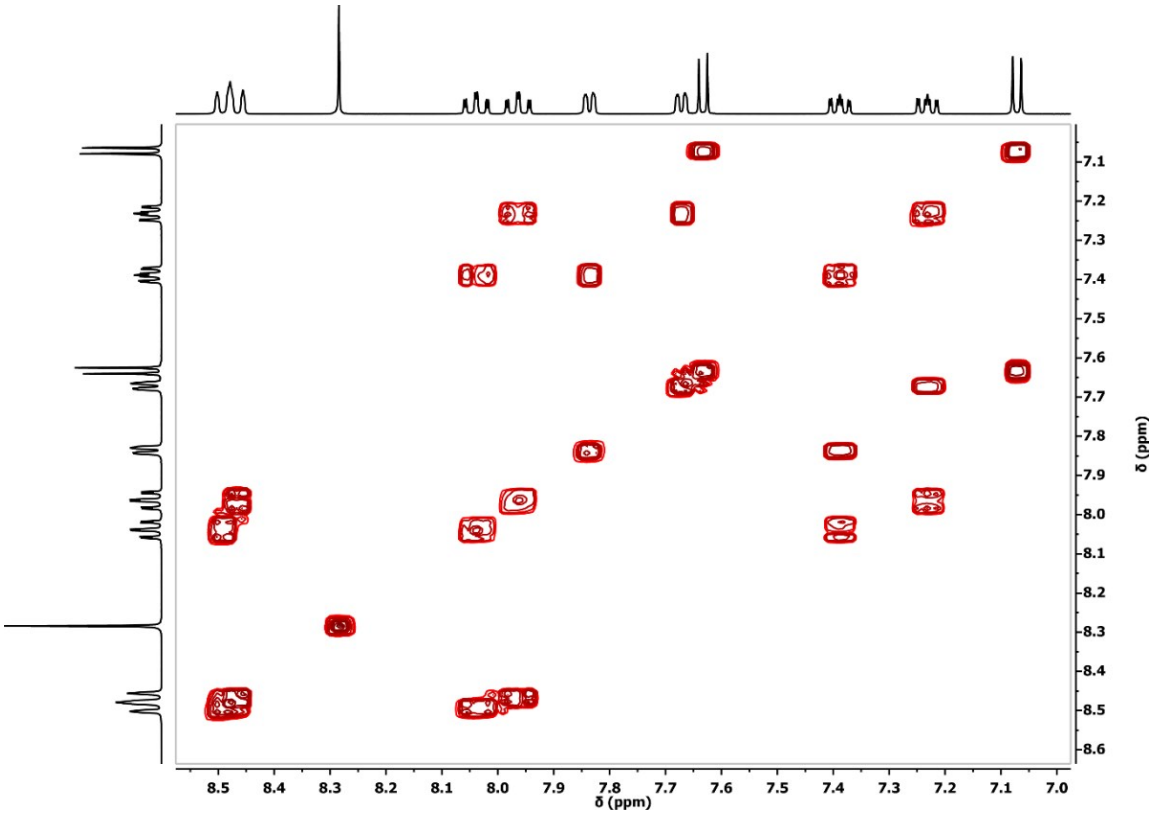

Figure S10. Partial ^{1}H-^{1}H COSY NMR spectrum of **2[PF$_6$]$_2$** in CD_3CN.

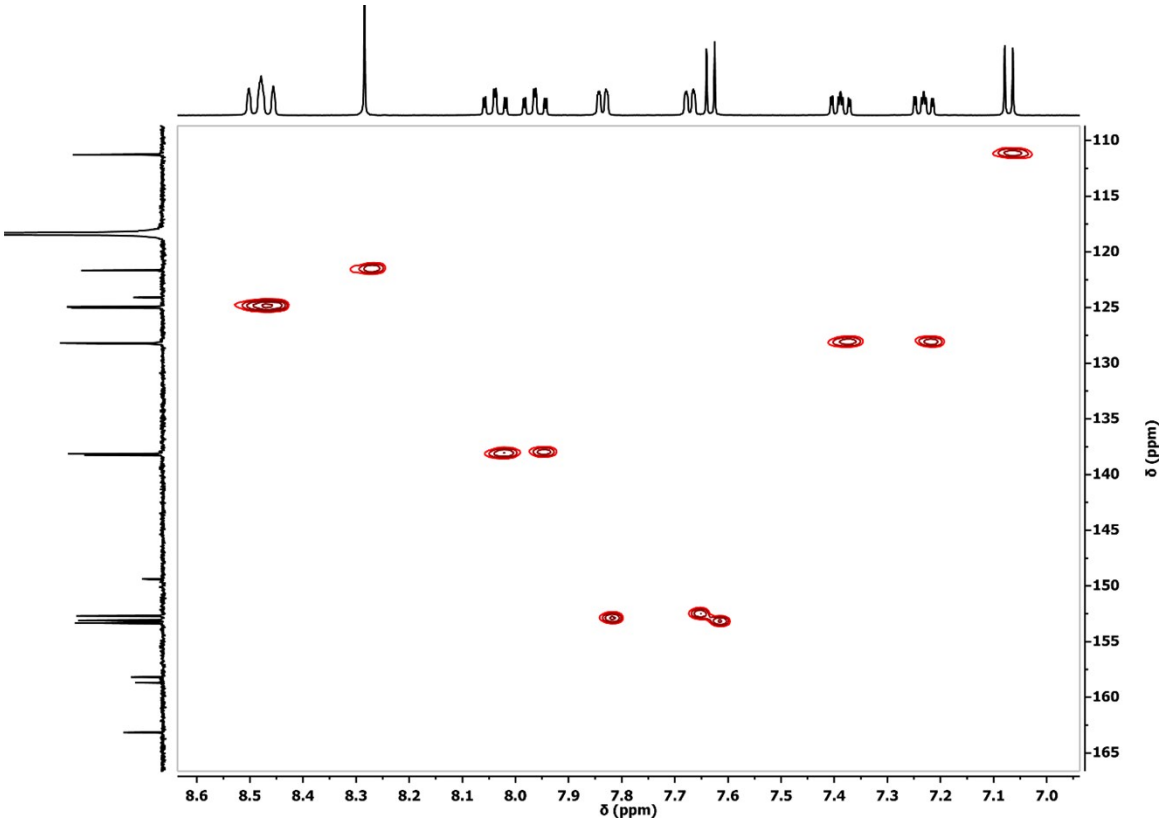

Figure S11. Partial ^{1}H-^{13}C HSQC NMR spectrum of **2[PF$_6$]$_2$** in CD_3CN.

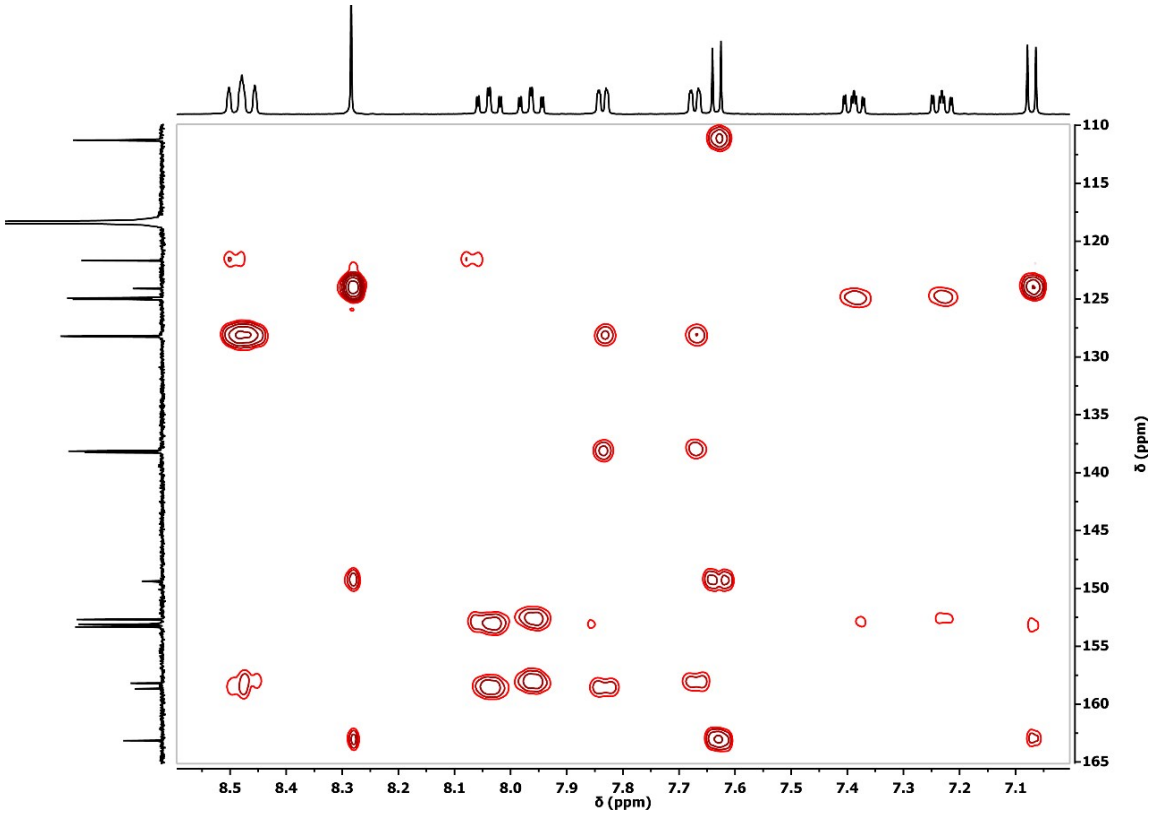

Figure S12. Partial ^{1}H-^{13}C HMBC NMR spectrum of **2[PF$_6$]$_2$** in CD_3CN.

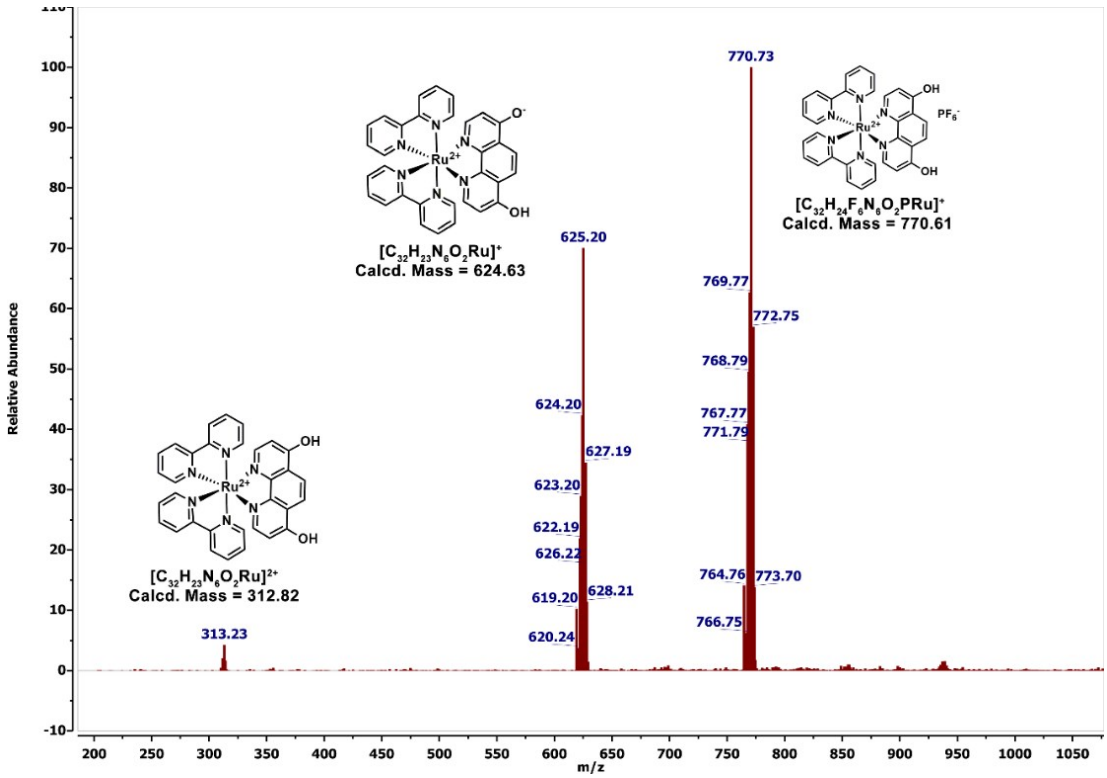

(a)

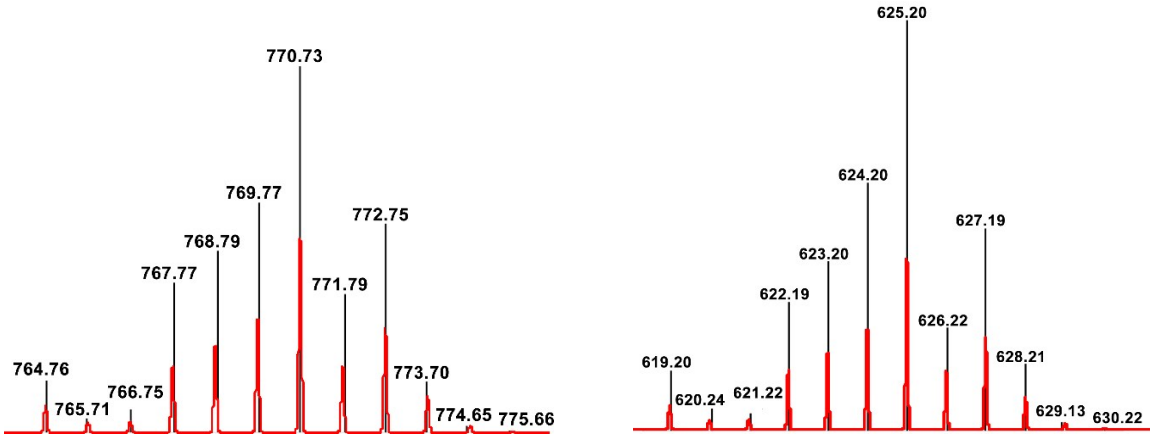

(b)

Figure S13. a) ESI-MS spectrum of **2[PF$_6$]$_2$** in CH_3CN and b) isotopic distribution of mass spectrum of **2[PF$_6$]$_2$** of experimentally obtained (black), simulated (red).

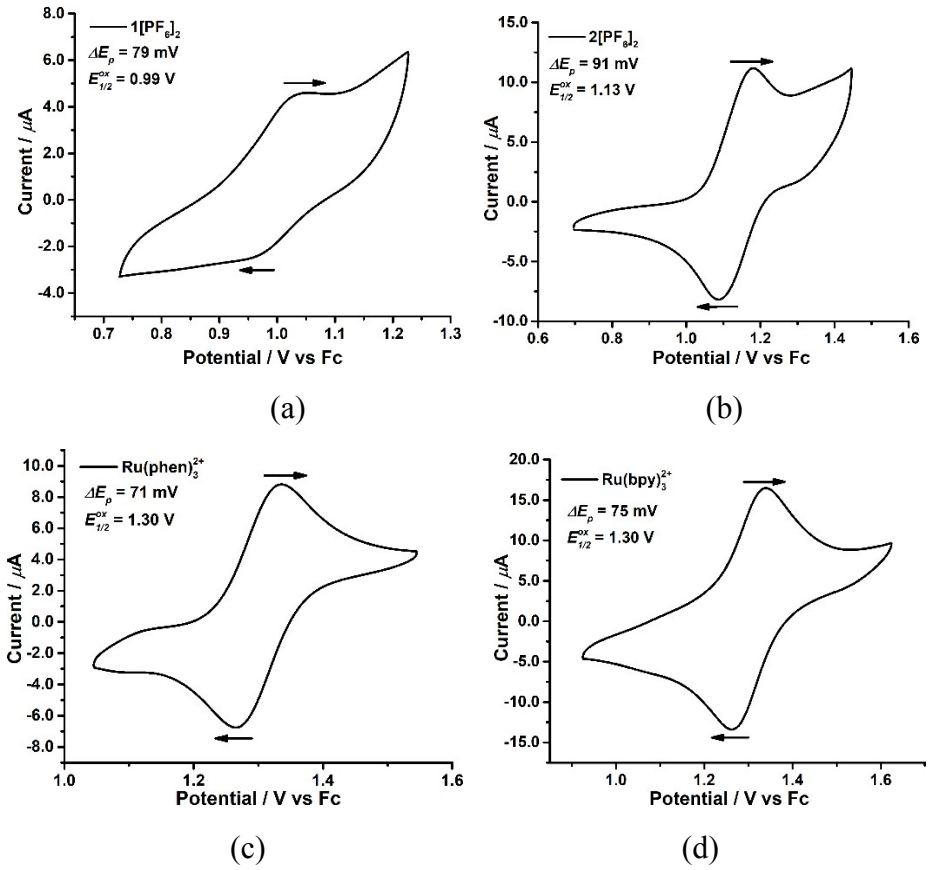

Figure S14. Cyclic voltammogram of 1.0 mM (a) **1[PF$_6$]$_2$**, (b) **2[PF$_6$]$_2$**, (c) [Ru(phen)$_3$](PF$_6$)$_2$ and (d) [Ru(bpy)$_3$](PF$_6$)$_2$ in dry and degassed acetonitrile in the presence of 0.1 M tetra-*n*-butylammonium perchlorate (Bu_4NClO_4) as a supporting electrolyte and potential axis was calibrated with Ferrocene.

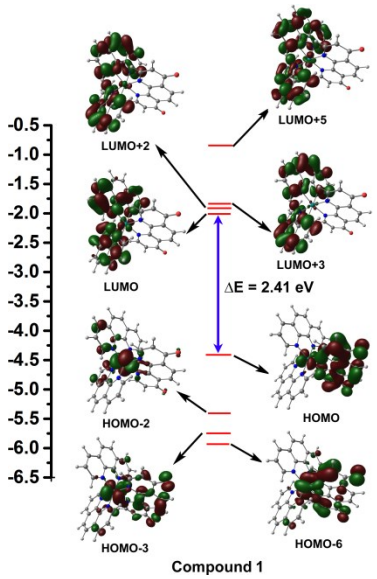

Figure S15. Energy level diagram obtained from TD-DFT (B3LYP/6-31G (d,p) // LANL2DZ) describing the dominant transitions that consisting of the ^{1}MLCT absorption band for compound **1** in water. [isovalue = 0.03].

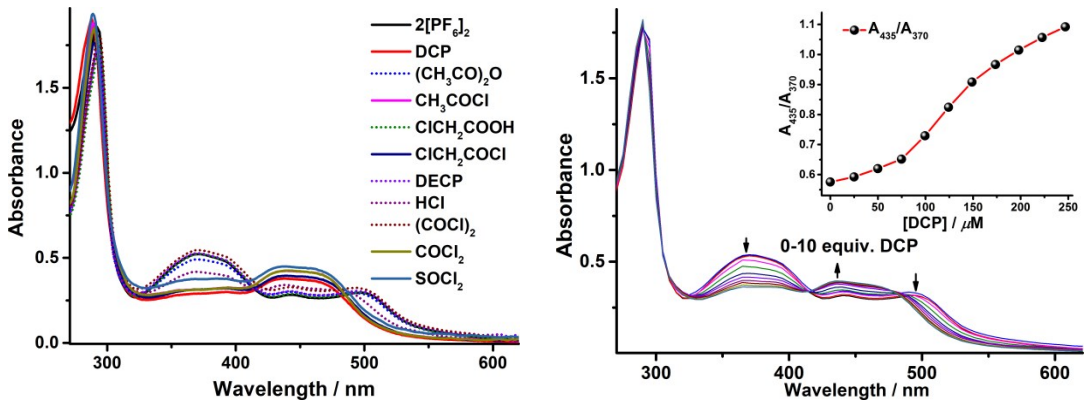

(a) (b)

Figure S16. (a) UV−vis selectivity of **2[PF$_6$]$_2$** with various analytes (10 equiv) in the presence of Et_3N (100 μM). (b) UV−vis titration of **2[PF$_6$]$_2$** upon gradual addition of DCP (0−0.25 mM) in the presence of Et_3N (100 μM) in aqueous-CH_3CN solution (H_2O: CH_3CN = 9:1, v/v) at 25 °C. ([probe] = 25 μM; Inset: plot of A_{435}/A_{370} vs concentration of DCP).

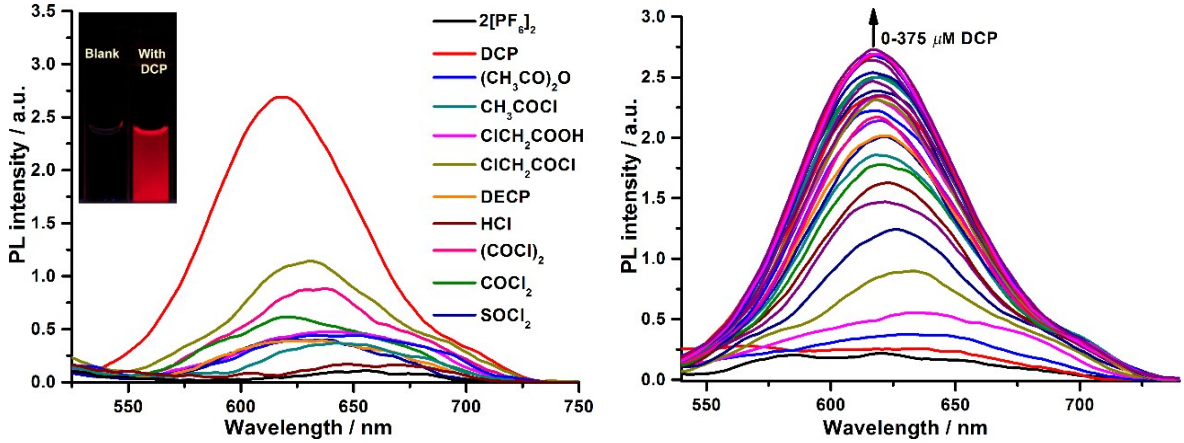

(a) (b)

Figure S17. (a) PL selectivity study of **2[PF$_6$]$_2$** upon addition of DCP and other competitive analytes (15 equiv.) in the presence of Et_3N (100 μM) in aqueous-CH_3CN solution (H_2O:CH_3CN; 9:1; v/v) at 25 ºC. *Inset:* photograph of probe in the absence/presence of DCP upon irradiation of UV light at 365 nm. (b) PL titration of **2[PF$_6$]$_2$** with DCP (0-375 μM) in the presence of Et_3N (100 μM) in aqueous-CH_3CN solution (H_2O:CH_3CN; 9:1; v/v) at 25 °C. ([probe] = 25 μM; λ_{ex} = 450 nm).

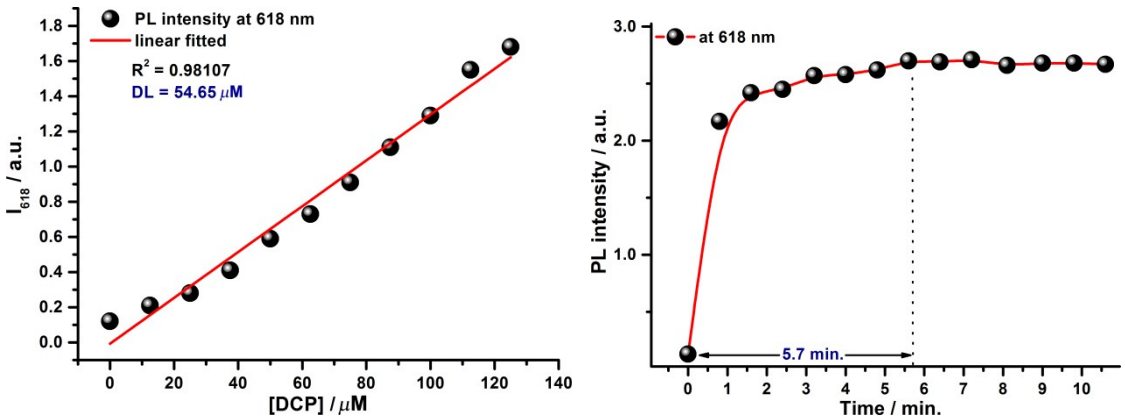

(a) (b)

Figure S18. (a) Calibration plot of **2[PF$_6$]$_2$** with DCP obtained from PL titration experiment over a concentration range 0−130 μM at 25 ºC. (b) Time course study of the PL response of **2[PF$_6$]$_2$** upon addition of 15 equiv. of DCP in the presence of Et_3N (100 μM) in aqueous-CH_3CN solution (H_2O:CH_3CN; 9:1; v/v) at 25 °C. ([probe] = 25 μM; λ_{ex} = 450 nm).

Determination of pK_a

The average pKa values of **1[PF$_6$]$_2$** and **2[PF$_6$]$_2$** were determined by UV-vis spectroscopic experiment of the complexes (25 μM) at different pH ranging from 1.7 to 9.0. The volume of 0.1 M Na_2HPO_4 and 0.1 M HCl has been varied to obtain a variety of pH solutions. The % changes in absorption at 490 nm for **1[PF$_6$]$_2$** (at 370 nm for **2[PF$_6$]$_2$**) was monitored with various pH and plotted against pH, which gave a sigmoid curve. The pK_a of an acid (HA) denotes the pH, where the concentration of the acid (HA) and its conjugate base (A^-) is equal. At the inflection point of the sigmoid curve, [HA] is nearly equal to the [A^-] and usually gives the pK_a value of the compound.

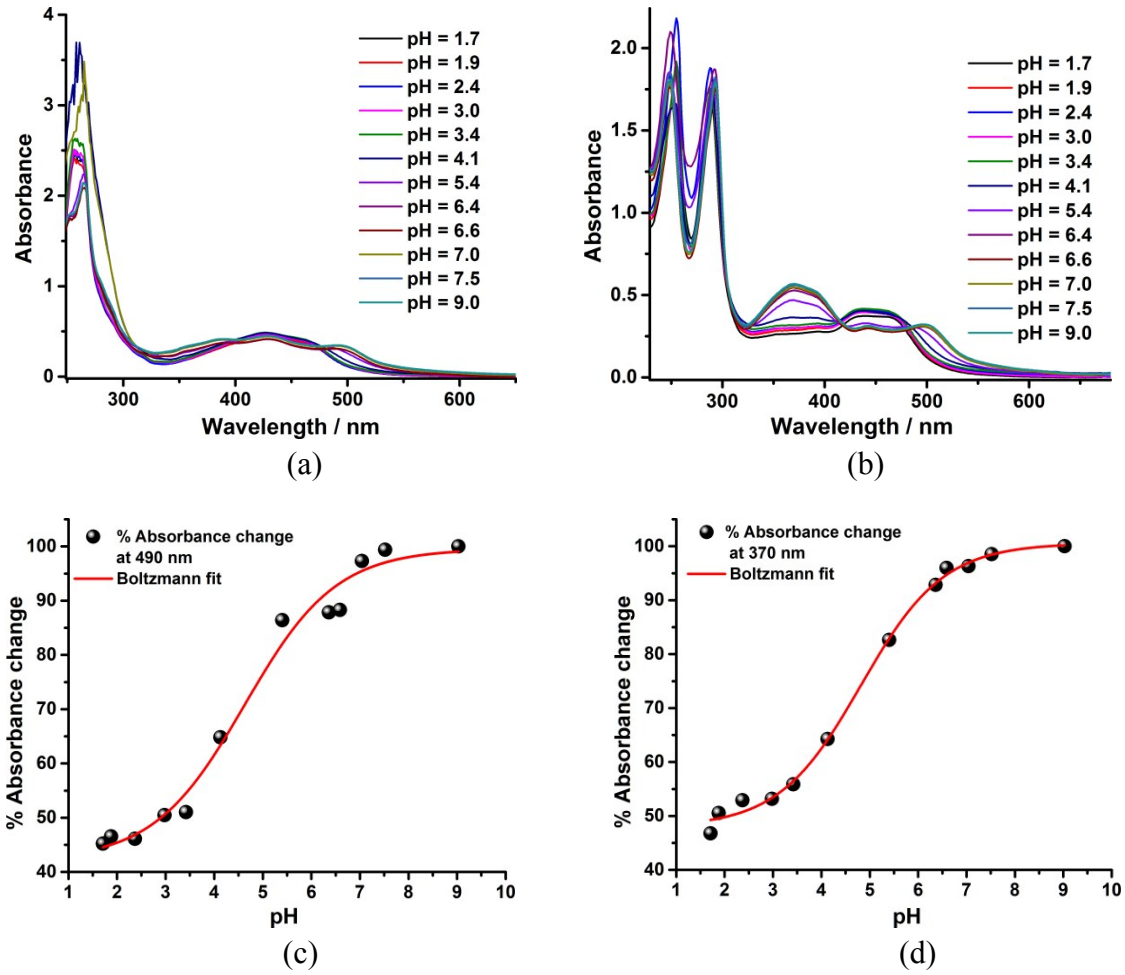

Figure S19. pH effect (1.7-9.0) on the UV-vis spectra of (a) **1[PF$_6$]$_2$** (25 μM) and (b) **2[PF$_6$]$_2$** (25 μM). (c) Plot of percent change in absorbance with pH (c) at 490 nm of **1[PF$_6$]$_2$** and (d) at 370 nm of **2[PF$_6$]$_2$**.

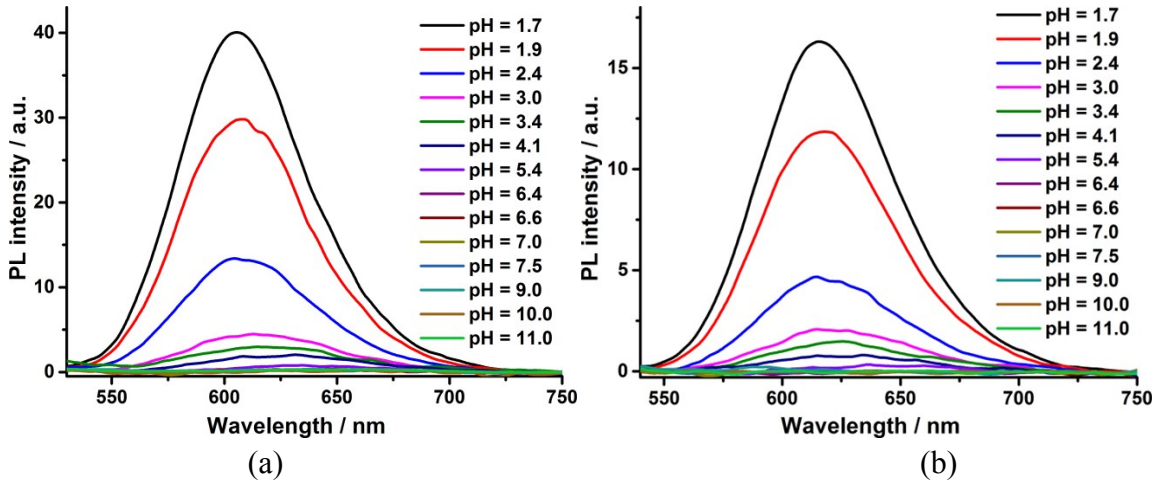

Figure S20. pH effect on the PL response of (a) **1[PF$_6$]$_2$** (25 μM) and (b) **2[PF$_6$]$_2$** (25 μM). (λ_{ex} = 450 nm; λ_{em} for compound **1[PF$_6$]$_2$** = 610 nm; λ_{em} for compound **2[PF$_6$]$_2$** = 618 nm).

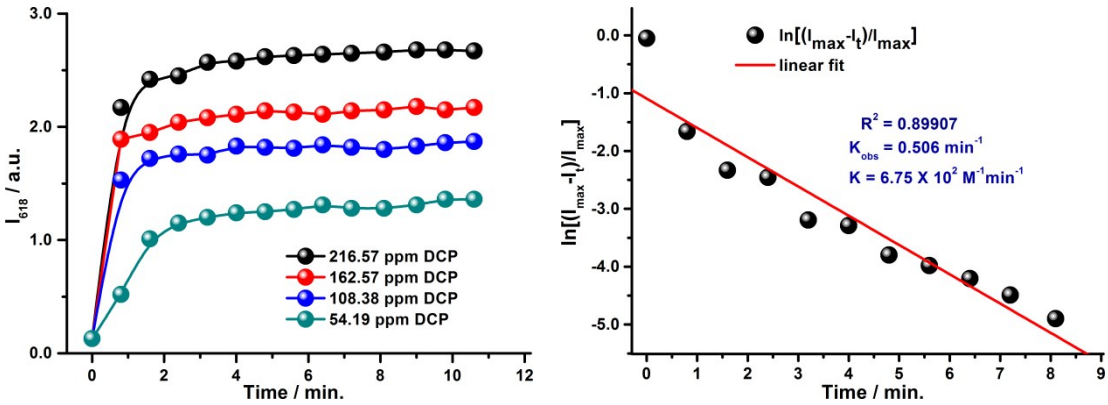

(a) (b)

Figure S21. (a) Pseudo first-order kinetic plot for the luminescence enhancement of **2[PF$_6$]$_2$** upon the reaction with DCP (54.19–216.57 ppm) in the presence of Et_3N (100 μM) in aqueous-CH_3CN solution (H_2O:CH_3CN; 9:1; v/v). (b) Linear correlation between $\ln[(I_{max}–I_t)/I_{max}$ and time obtained from the reaction of **2[PF$_6$]$_2$** with DCP (216.57 ppm). ([probe] = 25 μM, λ_{ex} = 450 nm and λ_{em} = 618 nm).

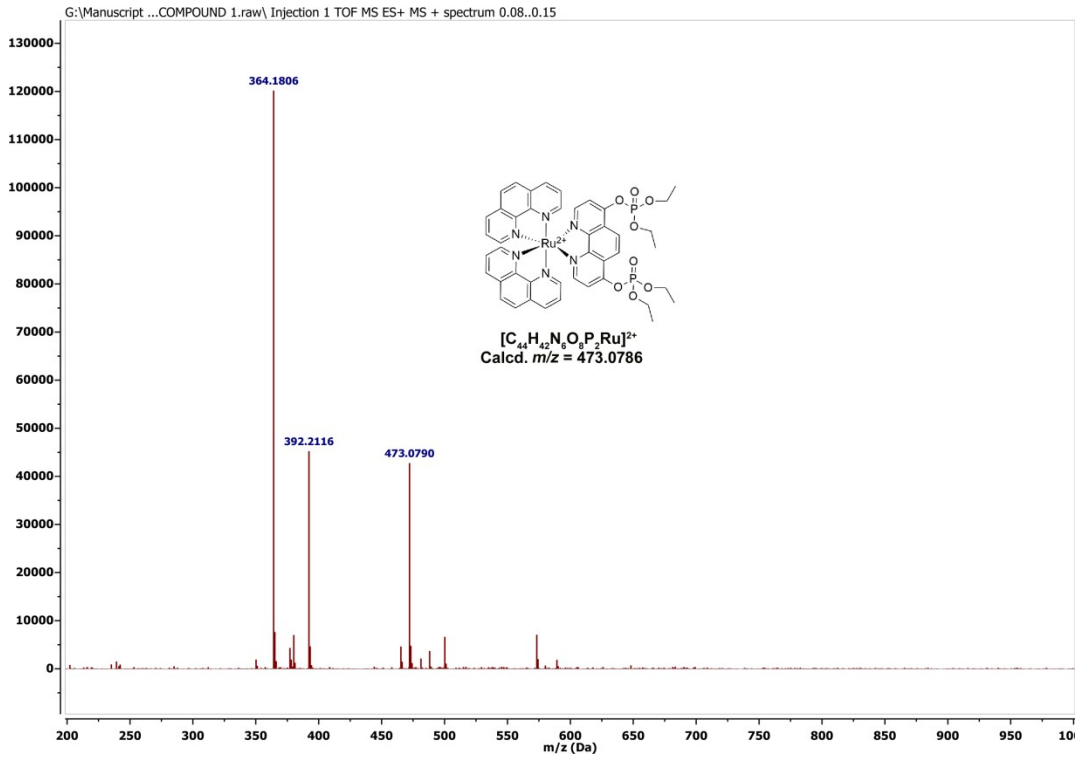

Figure S22. ESI-HRMS mass spectrum of a mixture of **1[PF$_6$]$_2$** (2.0 mM) and DCP (8.0 mM) in CH_3CN.

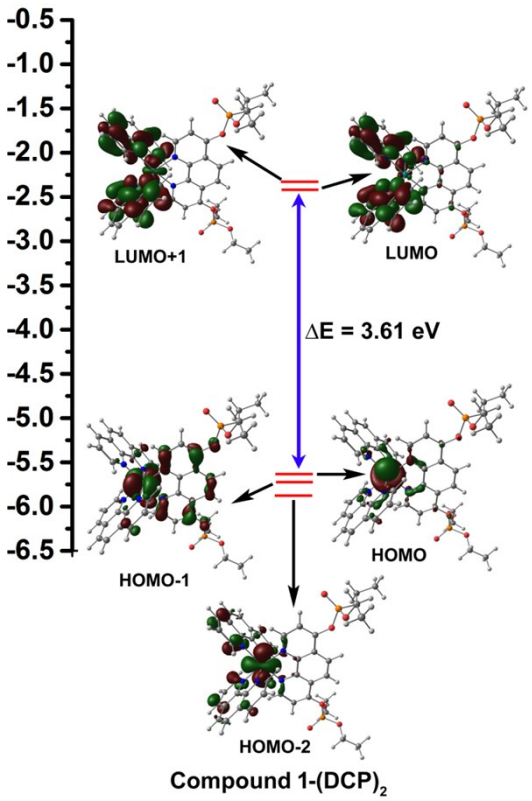

Figure S23. Energy level diagram obtained from TD-DFT (B3LYP/6-31G (d,p) // LANL2DZ) describing the dominant transitions that consisting of the ^{1}MLCT absorption band for compound **1-**$(DCP)_2$ in water. [isovalue = 0.03].

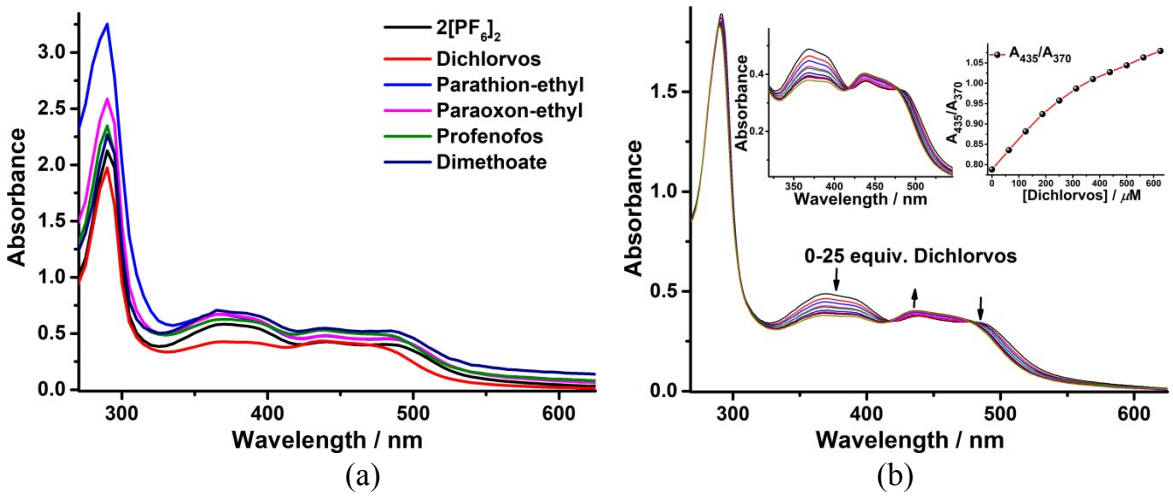

Figure S24. (a) UV−vis selectivity of **2[PF$_6$]$_2$** with various pesticides (25 equiv). (b) UV-vis titration of **2[PF$_6$]$_2$** upon gradual addition of Dichlorvos (0−625 μM) in the presence of Et_3N (100 μM) in aqueous-CH_3CN solution (H_2O: CH_3CN = 9:1, v/v) at 25 °C. ([probe] = 25 μM; *Inset*: plot of A_{435}/A_{370} vs concentration of Dichlorvos).

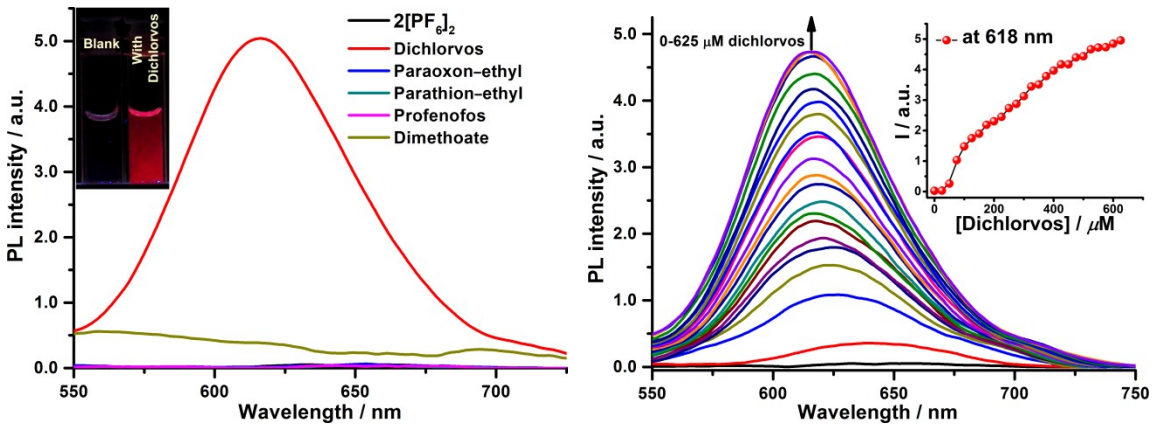

(a) (b)

Figure S25. (a) PL selectivity of **2[PF$_6$]$_2$** in presence of dichlorvos and other pesticides in the presence of Et_3N (100 μM) in aqueous-CH_3CN solution (H_2O:CH_3CN; 9:1; v/v) at 25 °C. Inset: photographs of probes with/without dichlorvos under UV irradiation (365 nm). (b) PL titration of **2[PF$_6$]$_2$** with dichlorvos (0–625 μM) in aqueous-CH_3CN solution (H_2O:CH_3CN; 9:1; v/v). Inset: Plot of PL intensity *vs* concentration of dichlorvos. ([probe] = 25 μM; λ_{ex} = 450 nm).

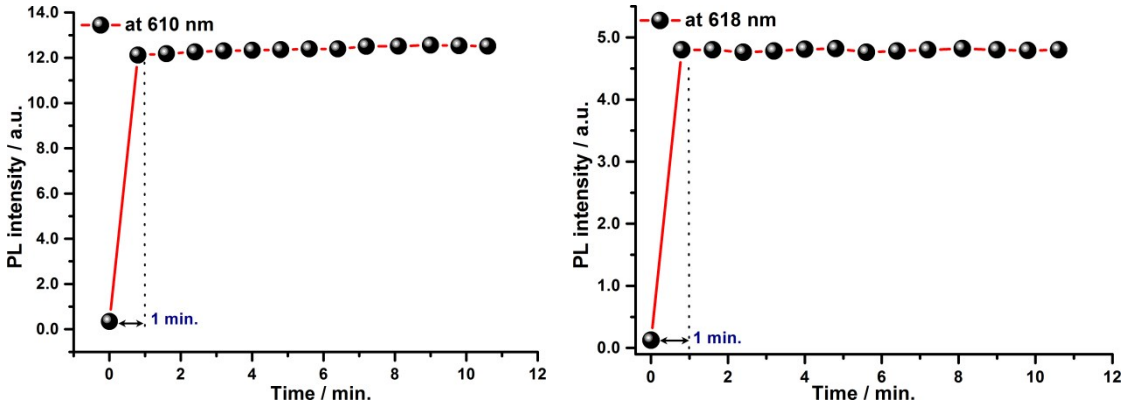

(a) (b)

Figure S26. PL intensity of (a) **1[PF$_6$]$_2$** and (b) **2[PF$_6$]$_2$** in presence of dichlorvos (25 equiv.) with time in the presence of Et_3N (100 μM) in aqueous-CH_3CN solution (H_2O: CH_3CN; 9:1; v/v). (λ_{ex} = 450 nm and λ_{em} = 610 nm for **1[PF$_6$]$_2$** and 618 nm for **2[PF$_6$]$_2$**).

Table S1. Crystal data and structure refinement for complex **1**.

Empirical formula	$C_{36}H_{28}N_6O_5Ru$	
Formula weight	725.71	
Temperature	293(2) K	
Wavelength	0.71073 Å	
Crystal system	Monoclinic	
Space group	*C* 2/c	
Unit cell dimensions	a = 27.2978(13) Å	α = 90°.
	b = 12.9642(6) Å	β = 95.730(5)°.
	c = 18.5018(9) Å	γ = 90°.
Volume	6515.0(5) $Å^3$	
Z	8	
Density (calculated)	1.480 Mg/m^3	
Absorption coefficient	0.534 mm^{-1}	
F(000)	2960	
Crystal size	0.240 x 0.180 x 0.100 mm^3	
Theta range for data collection	3.000 to 26.372°.	
Index ranges	-33<=h<=34, -14<=k<=16, -23<=l<=22	
Reflections collected	17750	
Independent reflections	6636 [R(int) = 0.0368]	
Completeness to theta = 25.242°	99.7 %	
Refinement method	Full-matrix least-squares on F^2	
Data / restraints / parameters	6636 / 0 / 423	
Goodness-of-fit on F^2	1.091	
Final R indices [I>2sigma(I)][a]	$R1$ = 0.0591, w$R2$ = 0.1778	
R indices (all data)[a]	$R1$ = 0.0791, w$R2$ = 0.1958	
Largest diff. peak and hole	1.361 and -0.562 e.$Å^{-3}$	

[a] $R1 = \Sigma||F_o| - |F_c||/\Sigma|F_o|$; $wR2 = \{\Sigma[w(F_o^2 - F_c^2)^2]/\Sigma w(F_o^2)^2\}^{1/2}$

Table S2. Crystal data and structure refinement for complex **2**.

Empirical formula	$C_{32}H_{22}F_6KN_6O_2PRu$	
Formula weight	807.69	
Temperature	293(2) K	
Wavelength	0.71073 Å	
Crystal system	Tetragonal	
Space group	$P4_2$/mbc	
Unit cell dimensions	a = 17.6705(11) Å	α = 90°.
	b = 17.6705(11) Å	β = 90°.
	c = 21.2817(18) Å	γ = 90°.
Volume	6645.1(10) $Å^3$	
Z	8	
Density (calculated)	1.615 Mg/m^3	
Absorption coefficient	0.719 mm^{-1}	
F(000)	3232	
Crystal size	0.210 x 0.140 x 0.100 mm^3	
Theta range for data collection	3.211 to 28.778°.	
Index ranges	-13<=h<=23, -14<=k<=21, -27<=l<=20	
Reflections collected	18230	
Independent reflections	4056 [R(int) = 0.1058]	
Completeness to theta = 26.000°	99.0 %	
Refinement method	Full-matrix least-squares on F^2	
Data / restraints / parameters	4056 / 1 / 239	
Goodness-of-fit on F^2	1.045	
Final R indices [I>2sigma(I)][a]	$R1$ = 0.1352, w$R2$ = 0.3178	
R indices (all data)[a]	$R1$ = 0.2062, w$R2$ = 0.3845	
Largest diff. peak and hole	1.787 and -1.283 e.$Å^{-3}$	

[a] $R1 = \Sigma||F_o| - |F_c||/\Sigma|F_o|$; $wR2 = \{\Sigma[w(F_o^2 - F_c^2)^2]/\Sigma w(F_o^2)^2\}^{1/2}$

Table S3. Selected bond lengths (Å) and angles (°) around the Ru(II) in complex **1.**

Bond lengths (Å)			
N(1)-Ru(1)	2.074(4)	N(2)-Ru(1)	2.076(4)
N(3)-Ru(1)	2.060(5)	N(4)-Ru(1)	2.045(4)
N(5)-Ru(1)	2.067(5)	N(6)-Ru(1)	2.052(5)
Bond angles (°)			
N(4)-Ru(1)-N(6)	92.02(18)	N(4)-Ru(1)-N(3)	80.24(17)
N(6)-Ru(1)-N(3)	169.21(17)	N(4)-Ru(1)-N(5)	91.96(17)
N(6)-Ru(1)-N(5)	79.91(19)	N(3)-Ru(1)-N(5)	92.76(18)
N(4)-Ru(1)-N(1)	94.19(16)	N(6)-Ru(1)-N(1)	96.11(18)
N(3)-Ru(1)-N(1)	91.97(17)	N(5)-Ru(1)-N(1)	172.80(17)
N(4)-Ru(1)-N(2)	170.24(18)	N(6)-Ru(1)-N(2)	95.56(18)
N(3)-Ru(1)-N(2)	93.00(18)	N(5)-Ru(1)-N(2)	95.41(17)
N(1)-Ru(1)-N(2)	78.92(17)		

Table S4. Selected bond lengths (Å) and angles (°) around the Ru(II) in complex **2.**

Bond lengths (Å)			
Ru(1)-N(2)[a]	2.034(11)	Ru(1)-N(2)	2.034(11)
Ru(1)-N(3)[a]	2.040(10)	Ru(1)-N(3)	2.040(10)
Ru(1)-N(1)[a]	2.068(10)	Ru(1)-N(1)	2.068(10)
Bond angles (°)			
N(2)[a]-Ru(1)-N(2)	176.7(6)	N(2)[a]-Ru(1)-N(3)[a]	98.0(4)
N(2)-Ru(1)-N(3)[a]	79.7(4)	N(2)[a]-Ru(1)-N(3)	79.7(4)
N(2)-Ru(1)-N(3)	98.0(4)	N(3)[a]-Ru(1)-N(3)	94.4(5)
N(2)[a]-Ru(1)-N(1)[a]	95.0(4)	N(2)-Ru(1)-N(1)[a]	87.5(4)
N(3)[a]-Ru(1)-N(1)[a]	93.2(4)	N(3)-Ru(1)-N(1)[a]	171.3(4)
N(2)[a]-Ru(1)-N(1)	87.5(4)	N(2)-Ru(1)-N(1)	95.0(4)
N(3)[a]-Ru(1)-N(1)	171.3(4)	N(3)-Ru(1)-N(1)	93.2(4)
N(1)[a]-Ru(1)-N(1)	79.6(5)		

Symmetry transformations used to generate equivalent atoms:

(a) 1/2 – y, 1/2 – x, 1/2 – z

Table S5. Selected singlet state electronic transitions obtained from TD-DFT calculation at B3LYP/6-31G (d,p) // LANL2DZ level of compound **1** and **1**-$(DCP)_2$ in water**.**

Complex	Experimentally observed transition (eV/nm)	Computed vertical excitation energy (eV/nm)	Composition	Oscillator strength (*f*)	Contribution (CI)
1	3.24 eV (382 nm)	3.31 eV (375 nm)	HOMO−3 → LUMO+3	0.05	33.0%
		3.21 eV (386 nm)	HOMO−6 → LUMO	0.07	53.5%
			HOMO → LUMO+5		12.4%
	2.88 eV (430 nm)	2.84 eV (437 nm)	HOMO-2→LUMO+2	0.04	62.1%
	2.53 eV (490 nm)	2.57 eV (482 nm)	HOMO−2→ LUMO	0.09	66.0%
1-$(DCP)_2$	2.88 eV (430 nm)	2.99 eV (415 nm)	HOMO−2 → LUMO	0.11	59.5%
			HOMO−1 → LUMO+1		27.7%
		2.89 eV (429 nm)	HOMO−1→ LUMO	0.01	66.4%